Highly Sensitive MoS$_2$ Humidity Sensors Array for Noncontact Sensation

Jing Zhao, Na Li, Hua Yu, Zheng Wei, Mengzhou Liao, Peng Chen, Shuopei Wang, Dongxia Shi, Qijun Sun,* and Guangyu Zhang*

Recently, 2D materials exhibit great potential for humidity sensing applications due to the fact that almost all atoms are at the surface. Therefore, the quality of the material surface becomes the key point for sensitive perception. This study reports an integrated, highly sensitive humidity sensors array based on large-area, uniform single-layer molybdenum disulfide with an ultraclean surface. Device mobilities and on/off ratios decrease linearly with the relative humidity varying from 0% to 35%, leading to a high sensitivity of more than 10^4. The reversible water physisorption process leads to short response and decay times. In addition, the device array on a flexible substrate shows stable performance, suggesting great potential in future noncontact interface localization applications.

Recently, flexible electronics have attracted considerable attention for their potential applications in displays, artificial skins, sensors, sustainable energy, etc.[1–10] Various touch-sensing devices have been reported and can easily detect the external stimuli through sensing the variations of their resistances or capacitances.[11–19] In certain circumstances, it is extremely important for such sensors to have the ability to sense without direct contact. Therefore, the moisture detection becomes a prominent approach to realize noncontact and long-range

Dr. J. Zhao, N. Li, H. Yu, Z. Wei, M. Z. Liao, P. Chen, S. P. Wang,
Prof. D. X. Shi, Prof. G. Y. Zhang
Beijing National Laboratory for Condensed Matter Physics,
Institute of Physics
Chinese Academy of Sciences
Beijing 100190, China
E-mail: gyzhang@aphy.iphy.ac.cn
Dr. J. Zhao, Prof. Q. Sun
Bejing Institute of Nanoenrgy and Nanosystems
Chinese Academy of Sciences, National Center for Nanoscience
and Technology (NCNST)
Beijing 100190, China
E-mail: sunqijun@binn.cas.cn
Dr. J. Zhao, N. Li, H. Yu, Z. Wei, M. Z. Liao, P. Chen, S. P. Wang,
Prof. D. X. Shi, Prof. G. Y. Zhang
School of Physical Sciences
University of Chinese Academy of Sciences
Beijing 100083, China
Prof. G. Y. Zhang
Collaborative Innovation Center of Quantum Matter
Beijing Key Laboratory for Nanomaterials and Nanodevices
Beijing 100190, China

signal induction.[20,21] In general, a high-performance humidity sensor requires the sensing material to have i) high surface to volume ratio, to effectively perceive the variation of humidity in the environment, and ii) interior competence, to interact with water molecules via physical absorption for repeatable utilization and short response times. Therefore, it is imperative to develop sensing materials bearing these two essential rules to achieve high-quality humidity sensors.

2D materials such as graphene have been widely studied for humidity sensing applications due to their high surface to volume ratios, excellent mechanical properties, outstanding flexibility, and high transparency.[12–26] For example, the resistance of graphene could change after adsorbing water molecules due to the doping effect. However, the resistance change is not abrupt, thereby resulting in a low sensitivity. Alternatively, graphene oxide (GO) or reduced graphene oxide (rGO) with functional groups show promise in achieving high sensitivity; however, it takes long time to recover their initial resistance state after suffering water molecules due to the formation of chemical bonds.[27,28] Compared with graphene, monolayer molybdenum disulfide (ML-MoS$_2$), being an important n-type semiconductor with excellent mechanical and electrical properties,[29,30] exhibits significant signal inductions with surface adsorbed water molecules.[31–33] Such ML-MoS$_2$-based high-performance humidity sensing devices are, in principle, promising building fundamental for flexible noncontact moisture mapping, but have not been demonstrated yet.

In this work, we report an integrated ML-MoS$_2$ humidity sensors array with remarkably high sensitivities for moisture mapping. These devices are fabricated from large-area continuous ML-MoS$_2$ films grown by chemical vapor deposition (CVD). In order to preserve the intrinsically high electronic quality of ML-MoS$_2$, we patterned the ML-MoS$_2$ films via an Au-assisted exfoliation technique.[34] The patterned ML-MoS$_2$ films with ultraclean surfaces, being a key for high sensitivities, eliminated the influence of contamination and passivation caused by RIE process. At appropriate gate modulations, the device resistances could have more than 10^4 Ω changes with the relative humidity (RH), varying from 0% to ≈35%—over 3 orders of magnitudes higher than the previously reported results. Besides, the sensitivity was observed to be tunable with applied different gate voltages from less than 10 to more than 10^4, which could satisfy different demands in various humidity sensing circumstances. A very short response/recovery time was also achieved,

**ADVANCED
SCIENCE NEWS**
www.advancedsciencenews.com

**ADVANCED
MATERIALS**
www.advmat.de

attributing to physisorption rather than chemical adsorption of water molecules on the MoS$_2$ surfaces. In addition, the reversible sensing properties allowed long lifespan of the fabricated MoS$_2$ humidity sensors (up to one month). Based on the as-fabricated devices array, we show a 3D color mapping of the humidity distribution with each pixel in the sensory array effectively indicating the relative humidity in high resolution. We also demonstrate the fabrication of such devices array on flexible polymer substrates, which represent comparable sensing performance to the devices on rigid Si wafer. The achieved large-area MoS$_2$ humidity sensor arrays with outstanding performances have great potential for noncontact sensation.

Figure 1a illustrates the fabrication process for a large area integrated ML-MoS$_2$ field effect transistor (FET) array. The uniform and continuous MoS$_2$ films were grown by CVD on heavily doped silicon substrate with 300-nm SiO$_2$. During the growth process, oxygen was introduced as a balance gas between the growth and etching so as to prevent multilayer growth and defects formation.[35] Au-assisted exfoliation technique was applied to obtain ultraclean and high-quality ML-MoS$_2$ patterns on the SiO$_2$/Si substrates.[34] Photolithograph, metal deposition (Ti/Au, 3/30 nm) and lifting-off techniques were performed to define the source–drain electrodes. An optical image of the 4 × 4 transistors array is shown in Figure 1b. The channel length and width are ≈25 and ≈50 µm, respectively. Barely no defect and contamination on the patterned MoS$_2$ surface can be observed by the atomic force microscope (AFM) scanning (Figure 1b). The ultraclean surface ensures efficient humidity sensing when the MoS$_2$ channels adsorb water molecules. Humidity sensing measurements were carried out in a vacuum chamber. Before measurements,
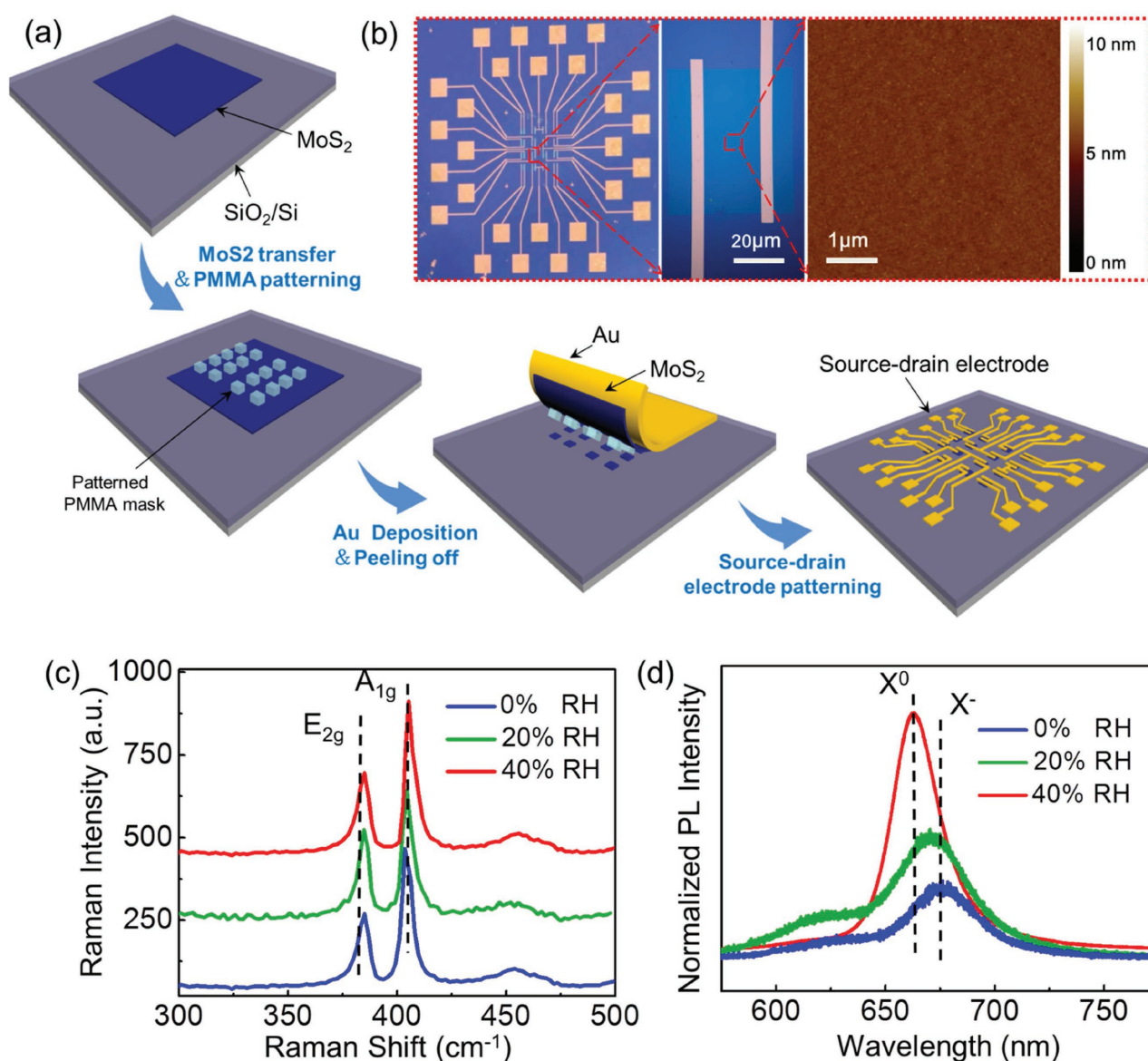

Figure 1. a) Schematic illustration of the fabrication process of monolayer MoS$_2$ FETs array. b) The optical image of the MoS$_2$ devices array on silicon substrate with 300-nm SiO$_2$, and the inset shows the AFM image of the patterned ultraclean MoS$_2$ surface. c,d) The Raman shift and PL spectrum of MoS$_2$ under different RHs (from 0% to 40%), respectively.

**ADVANCED
SCIENCE NEWS**
www.advancedsciencenews.com

**ADVANCED
MATERIALS**
www.advmat.de

the chamber was first pumped below a base pressure of $\approx 10^{-3}$ Torr. Water vapor carried out by nitrogen then flowed into the chamber, and the relative humidity (RH) could be precisely controlled through regulation of the nitrogen flow rate.

Optical properties of ML-MoS$_2$ under different RHs were first characterized. For pristine MoS$_2$ in the atmosphere environment, two typical Raman peaks E$_{2g}$ $\approx$ 384 cm^{-1} and A$_{1g}$ $\approx$ 404 cm^{-1} were observed (Figure S2, Supporting Information), which reflected the in-plane vibration and out-of-plane phonon coupling mode of MoS$_2$, respectively.[36] With the relative humidity varying from 0% to 40% (Figure 1c), the position of E$_{2g}$ peaks show no obvious change while the A$_{1g}$ peaks show a shift from $\approx$403.5 to $\approx$405.5 cm^{-1} due to the change of electron–phonon interactions caused by water molecules adsorption.[37,38] The photoluminescence (PL) spectrum of MoS$_2$ in Figure 1d at different RH conditions also displays the effect of water molecules adsorption. The two characteristic PL peaks at $\approx$1.88 eV (663 nm) and $\approx$1.84 eV (675 nm) are associated with the recombinations of neutral exciton (X^0) and negatively charged exciton (trion, X$^-$), respectively.[39] The adsorption of water molecules on MoS$_2$ film was considered as a reversible "molecular gating" force to deplete the excess electrons. Hence,

as the RH increased from 0% to 40%, the depletion of electrons by adsorbed water molecules activated the neutral exciton (X^0) recombination but diminishes X$^-$ recombination, represented as a $\approx$40 meV blue shift of PL peaks (Figure 1d). Besides, a dramatic enhancement in PL intensity was observed due to the activation of a new radiative recombination channel induced by electrons transferring from the ML-MoS$_2$ to water molecules. The enhanced PL intensity accompanied with peak shift for MoS$_2$ suffering water molecules is consistent with the previous calculations.[40,41] The observed PL modulation can further sustain the Raman characterization results and eliminate the substrate strain effect on influencing the A$_{1g}$ shift. Moreover, the Raman and PL spectrum could be restored to their initial states after vacuum pumping, indicating that water molecules adsorption is a physical instead of chemical process (Figure S3, Supporting Information). As a result, these reversible optical properties of monolayer MoS$_2$ reveals its potential application in robust and reusable humidity sensors.

Electrical properties of the as-fabricated ML-MoS$_2$ FETs were subsequently characterized. Before measurements, the MoS$_2$ FETs were first annealed at 450 K in vacuum to eliminate the surface adsorptions. **Figure 2**a shows the n-type
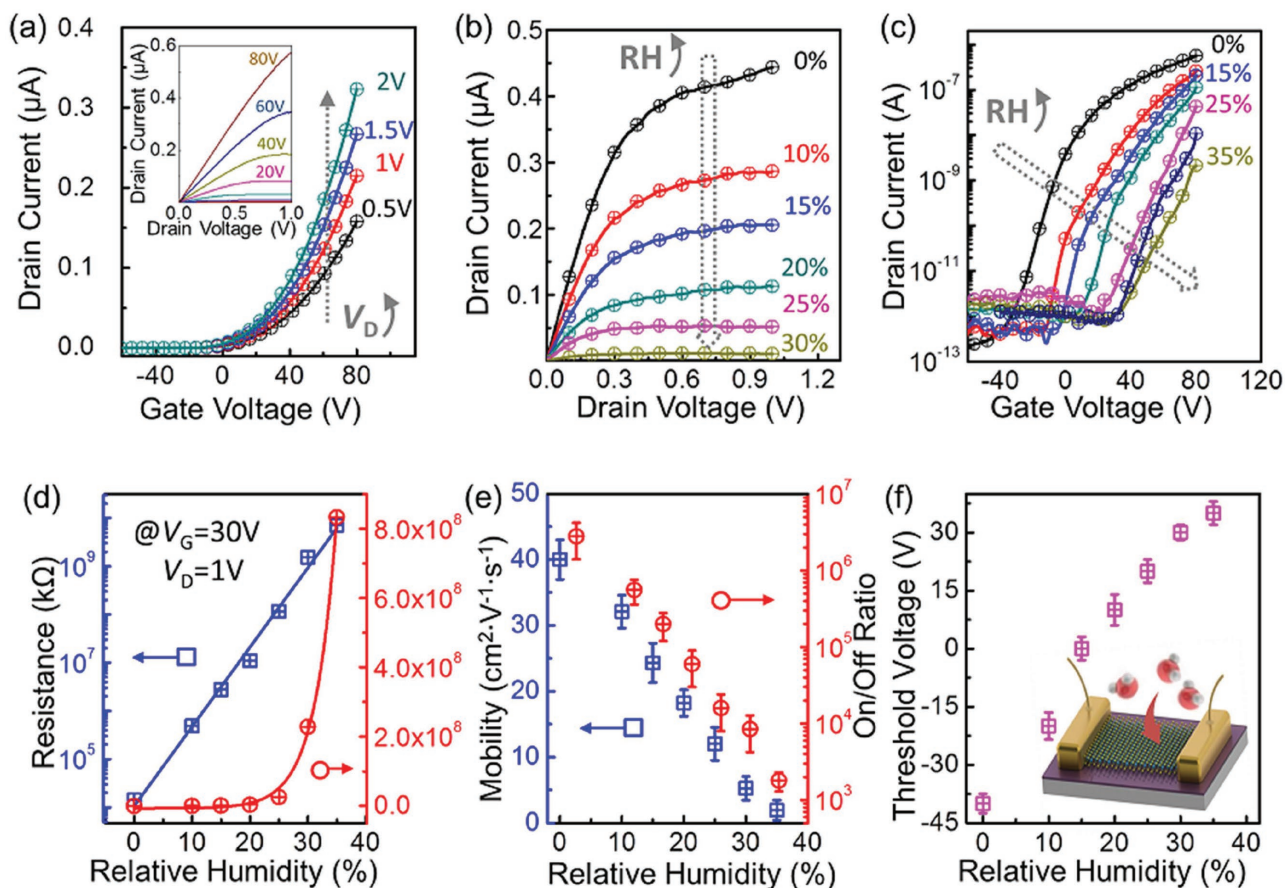
Figure 2. Electrical properties of the MoS$_2$ FET under different RHs. a) The typical transport property of the MoS$_2$ FET at 0% RH. b) The output characteristic of the MoS$_2$ FET under different RHs with the gate voltage at 80 V. c) The transfer curves of the device with RHs increasing from 0% to 35% (V_D = 1 V). d) The resistance variation at different RHs (V_G = 30 V), the blue and red lines show increment trends in linear and logarithmic coordinates, respectively. e) The statistical results for mobilities and on/off ratios, which decrease in a linear relation with RH increments. f) The threshold voltages shift to positive direction with increased RHs due to the enhanced doping level by adsorbed water molecules.

**ADVANCED
SCIENCE NEWS**
www.advancedsciencenews.com

**ADVANCED
MATERIALS**
www.advmat.de

transport characteristics of a typical device which was measured in a vacuum probe station by semiconductor analysis system (Agilent 4156C). Linear output properties of the device at low bias voltages (the inset image in Figure 2a) were obtained, indicating good ohmic contact between MoS_2 and source–drain electrodes. At a source–drain voltage (V_D) of 1 V, the on/off ratio can reach ≈10^6 and the calculated mobility of the device is ≈40 cm^2 V^{-1} s^{-1}. Output characteristics of the device under different RHs are shown in Figure 2b. With the RHs varying from 0% to 30%, the saturated source–drain currents (I_D) show strong modulation effect from 11 to 440 nA at a gate voltage (V_G) of 80 V. The linear region (V_D < 0.3 V) of I_D–V_D curves represented that the RH variations had almost no influences on the ohmic contact between source–drain electrodes and MoS_2 channel. Therefore, the increased channel resistance under higher RHs in this work was not induced by the Schottky barrier modulation as demonstrated in previous report.[31] Figure 2c illustrates the transfer curves of MoS_2 FET at different RHs from 0% to 35%, in which V_D was kept at 1 V while the V_G was scanned from −80 to 80 V. When the RHs increased from 0% to 35%, the curves showed significant positive shift. The current at V_G = 80 V displayed remarkable decrements under increased RHs. On the contrary, the currents at the off state (the lowest current position in each transfer curve showed slight increments.

The calculated resistance of MoS_2 has a linear relationship with increased RHs in logarithmic coordinates (left curve in Figure 2d), which reflects the actual variation of the channel resistance in an exponential increment manner due to the modulation of charge density by adsorbed water molecules. The resistance of MoS_2 FET in Figure 2d is extracted to be 1.27 × 10^7 Ω in dry air (RH = 0%), and it increases to ≈8.3 × 10^{11} Ω under RH = 35% at V_G = 30 V. The achieved >10^4 Ω resistance variation is attributed to the effective adsorption of water molecules on the patterned ultraclean MoS_2 surface. Notably, the sensitivity, defined as $\Delta R/R_0$, can be modulated by V_G and the detailed results are illustrated in Figure S4a (Supporting Information). As shown in Figure S4b (Supporting Information), when the gate voltage increased from −10 to 80 V, the sensitivities show a parabolic shape and can reach 10^4 at V_G = 30 V. This >4 orders of resistance magnitude change indicate the ultrahigh sensitivity in this work compared with previously reported MoS_2-based chemical sensors.[31–33] The gate modulated sensitivity in these MoS_2 humidity sensors could also be beneficial and may satisfy various needs in different sensing conditions, making them more competitive than graphene-based humidity sensors. The gate modulated sensitivity in these MoS_2 humidity sensors could also be beneficial and may satisfy various needs in different sensing conditions. The sensing limitation of RH is around 40% at V_G = 30 V (Figure S5, Supporting Information), over which MoS_2 resistance are too large to be detectable. However, we can increase this sensing range above 40% when increasing the gate voltages larger than 30 V (as shown in Figure S4 in the Supporting Information) by sacrificing the humidity sensitivities. We measured more than 50 devices with different channel lengths and widths and the statistic data is shown in Figure 2e, revealing a very stable and reliable sensing behavior. Besides, the threshold voltages of these devices tend to shift

from negative to positive direction with the increased RHs (Figure 2f). We attribute this phenomenon to more electrons transfer from MoS_2 to the adsorbed molecules at increased RHs. Therefore, the main reason for the non-negligible change of the electrical performance can be attributed to the enhanced doping effect of adsorbed water molecules on MoS_2 surface with increased RHs, which is consistent with the above Raman and PL analysis.

Apart from the sensitivity measurements, dynamic tests of RHs sensation were also carried out to provide the time-responsive characteristics. During tests, pulsed water vapor was introduced into the measurement chamber, in which the RHs can be precisely controlled through a solenoid valve. The estimated pulse width is below 1 s. **Figure 3**a shows the time-evolution of a device's resistance measured at V_G = 30 V and V_D = 1 V under different water vapor pulses, exhibiting the quick response of the device. As shown in Figure 3b, after the water vapor was pumped out, the resistance can recover to its original value immediately, representing the reproducible and stable humidity sensing performance. Within a single cycle, the response and recovery time were extracted to be ≈10 and ≈60 s, respectively (Figure 3c), which were faster than most of the reported humidity sensors based on 2D materials.[42,43] This short recover time and restorable performance of our devices confirm the importance of ultraclean surfaces compared with the previous study based on MoS_2.[33] Remarkably, resistances of our MoS_2 devices (V_G = 80 V, V_D = 1 V) are capable of being maintained at a fixed RH over a month (Figure 3d), indicating excellent stability and durability.

Based on these highly sensitive and rapidly responsive humidity sensing devices, we fabricated integrated devices array for detection of the moisture distribution in external environments. **Figure 4**a shows the as-fabricated 6 × 6 devices array on the SiO_2/Si substrate. As an illustration, a human finger treated as a moist source was gradually approaching the devices array. Individual device can be regarded as one pixel, and its resistance at V_G = 30 V and V_D = 1 V shows exponentially relationship to the finger-device distances (Figure 4b). Therefore, the devices array can monitor the relative humidity distribution in real time according to the resistance changes. The left image in Figure 4c reveals the normalized resistance changes of each device in the sensory array upon finger approaching. According to Figure 2d, the distribution of RHs shown in Figure 4c can be deduced from the normalized resistance changes in the left image. To further demonstrate the high resolution sensing ability of integrated humidity sensors, we thus used an "N" shaped moist object to approach the devices array and we were able to identify this "N" shape in the humidity mapping image (Figure 4d). The demonstrated noncontact humidity sensing property offers great opportunity for using such highly sensitive MoS_2 FETs array for long range interaction or localization applications.

These MoS_2-based sensors can be also fabricated on flexible substrates which would broaden their application fields. Here we used a soft polydimethylsiloxane (PDMS) as the substrate. As shown in Figure 4e, indium tin oxides (ITO) and aluminum oxide were used as bottom gate electrode and dielectric layer, respectively. MoS_2 films were first transferred onto the flexible substrates and the later-on device fabrication process was

ADVANCED
SCIENCE NEWS
www.advancedsciencenews.com

ADVANCED
MATERIALS
www.advmat.de
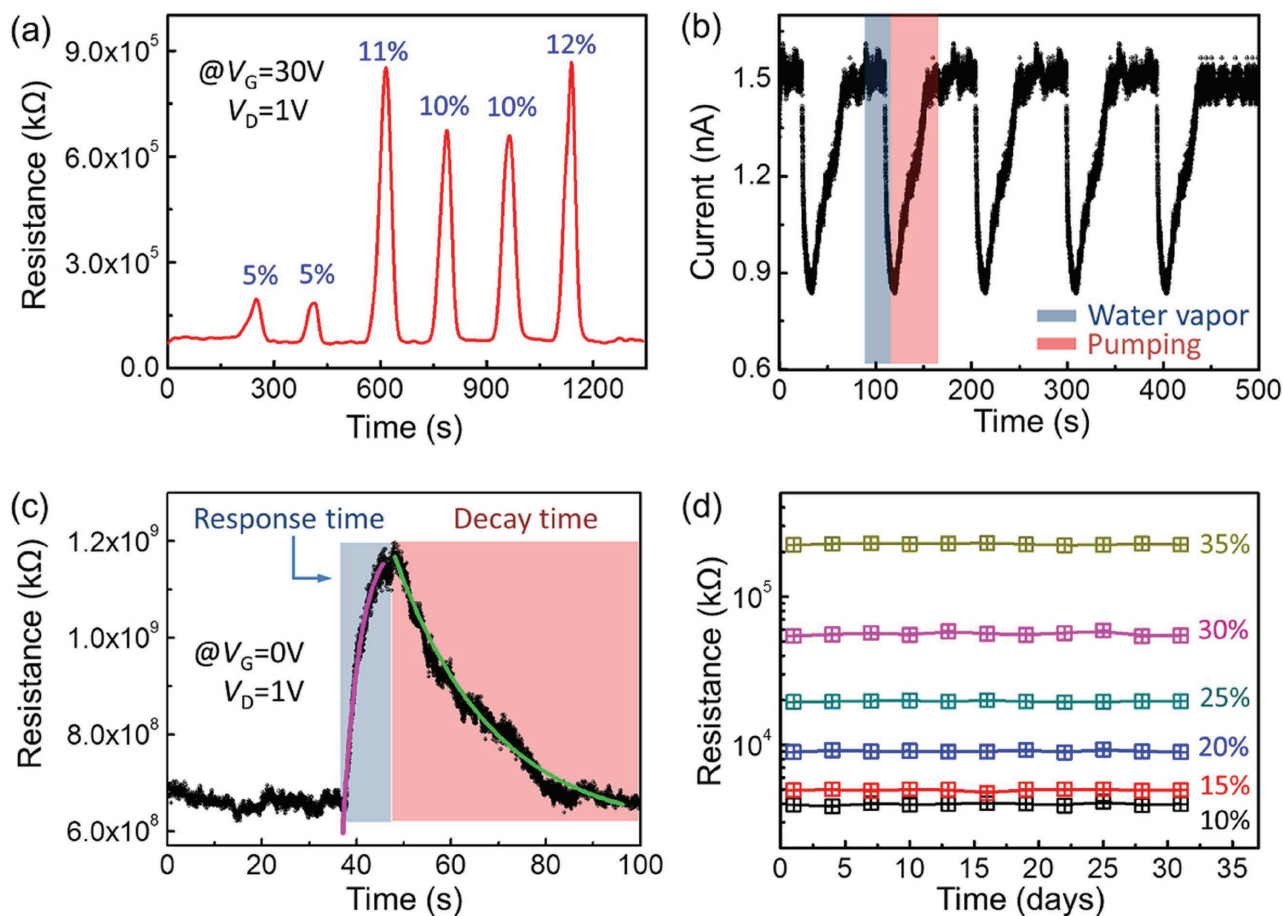
Figure 3. Real-time characterization of the MoS$_2$ humidity sensor. a) The real-time test of the resistance change versus different RHs. b) Dynamic stability test of the humidity sensor under the RH at 10%. c) Response time analysis extracted from one cycle of RH pulse in (b). According to the fitting line, the response time and decay time is ≈10 and ≈60 s, respectively. d) Long-term stability test of the humidity sensor under different RHs. The device shows ultrahigh stability for humidity sensing even after one month measurement.

similar to those described above. These devices on PDMS substrates show high performances (Figure S7, Supporting Information) and immunity upon bending (Figure S8, Supporting Information).[44] Humidity sensing tests on these devices were also carried out under both flat and bent (strain ≈1%) conditions (Figure 4f), showing similar sensing behavior, which would provide broad prospects for applications in multifunctional flexible electronics.

In conclusion, high performance humidity sensors array based on integrated MoS$_2$ FETs was demonstrated. The optical characteristics of monolayer MoS$_2$ film were remarkably affected by RH changes in external environment. The blue shifts of A$_{1g}$ in Raman shift and enhanced PL intensity represented the p-type doping effect caused by water molecules. The resistance of MoS$_2$ FET greatly increased in an exponential manner with RH varying from 0% to 35%. The sensitivity can be tuned by applied gate voltages and the highest value more than 10^4, the best ever reported for MoS$_2$ humidity sensors, has been achieved. In addition to the high sensitivity, these devices also showed fast response/recovery time and long-term stability. Integrated sensor array was demonstrated for noncontact mapping of the distribution of RHs. It can be used in future

untouched switches to decrease the risk of bacterial transmission, localization systems, and so on. The fabricated MoS$_2$ humidity sensor is believed to possess great potential in long term and reusable humidity sensing applications.

Experimental Section

Monolayer MoS$_2$ Synthesis: The wafer scale monolayer MoS$_2$ film was synthesized in a CVD system with three temperature zones. The growth precursors were sulfur (S) (Alfa Aesar 99.9%) and molybdenum trioxide (MoO$_3$) (Alfa Aesar 99.999%), which were loaded in zone I and II, respectively. The substrate was loaded in zone III. The working temperature of three temperature zones was 115, 560, and 800 °C. In the growth process, 100 sccm Ar was utilized as carrier gas and the pressure was kept at 1.0 Torr. After 10 min deposition, the substrate could be covered with monolayer MoS$_2$. Then the furnace was cooled down slowly to room temperature to take out the sample.

Raman Shift and PL Spectrum Measurement: Micro-Raman shift and PL measurements were performed on a JY Horiba HR800 system. The emission laser (spot size is around 1 μm) had a wavelength of 532 nm with power at 0.6 mW. A 50× objective lens was used for laser focusing and signal collecting with long working distance in order to focus on the MoS$_2$ sample in the vacuum chamber. Under different RH conditions,
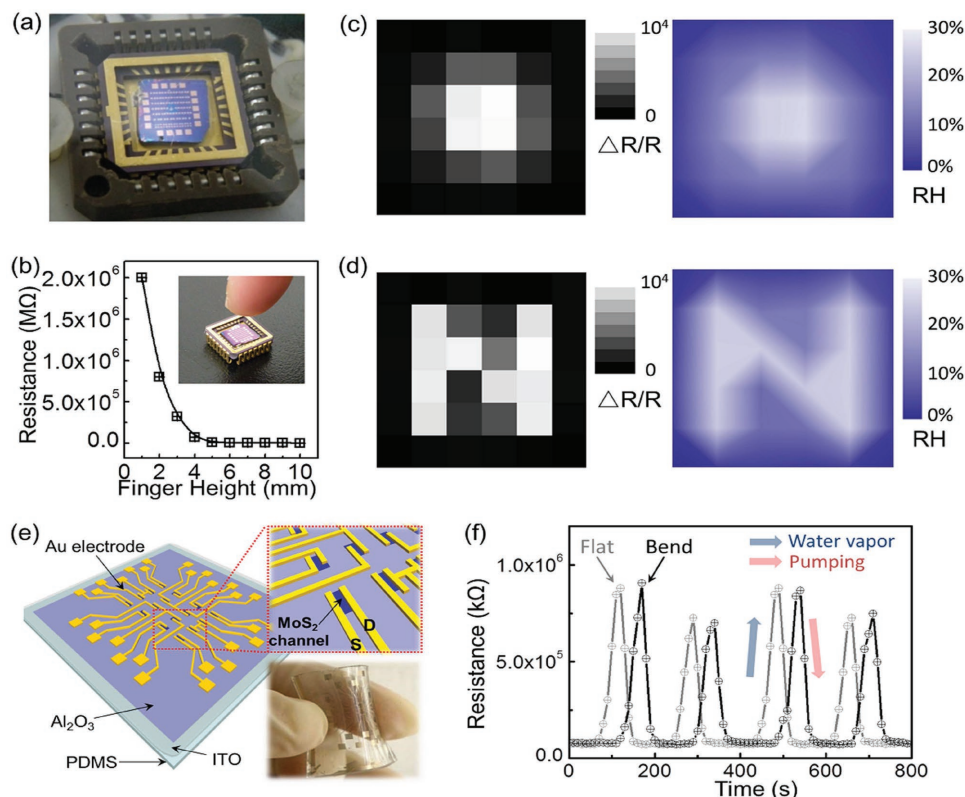
Figure 4. Demonstration of the noncontact humidity sensing properties with the integrated MoS_2 FETs array on both rigid and soft substrates. a) The optical image of the MoS_2 humidity sensor array in the chip carrier. b) The resistance increased exponentially with the finger moving closer to the MoS_2 device. c) The left image shows the measured resistances of each MoS_2 FET pixel when the finger has a certain distance (3 mm) from the sensory array. The source–drain and gate voltages are kept at 1 and 30 V, respectively. The right image shows the calculated RH distribution according to the measured sensing results (resistance changes vs RHs). d) The distributions of resistances and calculated RHs according to a wet object in "N" shape with a distance (3 mm) with the sensory array. e) Schematic illustration of MoS_2 FETs array on soft PDMS substrate. Insets show the magnified MoS_2 channels and optical image of the sensory array, respectively. f) The real-time humidity sensing tests of the MoS_2 FET on both flat and bend (strain ≈1%) condition ($V_G = 10$ V, $V_D = 3$ V). Similar sensing performance was observed.

Raman and PL spectra of more than 20 spots in 1×1 cm^2 area were collected to reduce the measurement errors.

MoS_2 Device Fabrication: For the MoS_2 FET on SiO_2/Si substrate, the photoresist (S1813) was prepared on MoS_2 surface by spin coating at 4000 rpm. After baking at 115 °C for 1 min to remove the solvent, the photoresist was patterned by UV-lithography (MA6, Karl Suss). Au film (20 nm) as the auxiliary layer was deposited on MoS_2 by the electron beam (e-beam) evaporation system. The thermal release tape was then attached to the surface of the sample gently. After removing the bubbles, MoS_2 without photoresist protecting and the photoresist mask patterns on MoS_2 were both detached from the substrate through peeling off the tape. Therefore, the desired MoS_2 patterns protected by photoresist could be left. Without RIE process, which generally caused contamination, the obtained MoS_2 patterns through Au-assisted peel-off method had an ultraclean surface. 3-nm Ti/30-nm Au was then deposited as source–drain electrodes via lift-off process followed by the second UV-lithography.

For the MoS_2 FET on soft PDMS, the 50-nm ITO was first deposited on the PDMS by the megnetron sputtering system. Then, the 60-nm thickness dielectric layer (Al_2O_3) was deposited by atomic layer deposition (ALD) at 110 °C using Savannah-100 system (Cambridge NanoTech. Inc.). In the ALD process, the H_2O (heated to 80 °C) and trimethyl aluminum (TMA) (at room temperature) were used as precursors. 20 sccm high purity N_2 was used as the carry gas. The TMA and H_2O were inlet in turn and the pulse time for TMA and H_2O were 0.015 and 0.15 s, respectively. The retention time lasted for 20 s for both precursors. The deposition rate was ≈0.9 Å per cycle. After the dielectric

layer being prepared, the grown MoS_2 was transferred on the surface by the standard wet transfer process. The patterning of MoS_2 channels and deposition of source–drain electrodes were subsequently conducted following the same fabrication process with that on Si substrate.

Device Measurement: To measure the MoS_2 FETs under different humidity conditions, the device was put on the chip carrier in vacuum chamber and bonded it out using Au thread. The chip carrier was connected to external measurement equipment (semiconductor analysis system, Agilent 4156C). Through controlling the gas flow, different RH conditions were obtained, which can be calibrated by the commercial humidity sensor. For real-time testing the electrical properties of the devices suffering humidity pulses, solenoid valve to accurately control the amount of water molecules was used.

Supporting Information

Supporting Information is available from the Wiley Online Library or from the author.

Acknowledgements

Conflict of Interest

The authors declare no conflict of interest.

Keywords

doping effect, high sensitivity, humidity sensor, molybdenum disulfide, physical adsorption

[1] B. Geffroy, P. LeRoy, C. Prat, *Polym. Int.* **2006**, *55*, 572.

[2] B. S. Ong, Y. L. Wu, P. Liu, S. Gardner, *J. Am. Chem. Soc.* **2004**, *126*, 3378.

[3] P. Liu, Y. L. Wu, Y. N. Li, B. S. Ong, S. P. Zhu, *J. Am. Chem. Soc.* **2006**, *128*, 4554.

[4] W. Zeng, L. Shu, Q. Li, S. Chen, F. Wang, X. M. Tao, *Adv. Mater.* **2014**, *26*, 5310.

[5] M. L. Hammock, A. Chortos, B. C. K. Tee, J. B. H. Tok, Z. N. Bao, *Adv. Mater.* **2013**, *25*, 5997.

[6] B. C. K. Tee, C. Wang, R. Allen, Z. N. Bao, *Nat. Nanotechnol.* **2012**, *7*, 825.

[7] D. H. Kim, N. S. Lu, R. Ma, Y. S. Kim, R. H. Kim, S. D. Wang, J. Wu, S. M. Won, H. Tao, A. Islam, K. J. Yu, T. I. Kim, R. Chowdhury, M. Ying, L. Z. Xu, M. Li, H. J. Chung, H. Keum, M. McCormick, P. Liu, Y. W. Zhang, F. G. Omenetto, Y. G. Huang, T. Coleman, J. A. Rogers, *Science* **2011**, *333*, 838.

[8] M. Kaltenbrunner, T. Sekitani, J. Reeder, T. Yokota, K. Kuribara, T. Tokuhara, M. Drack, R. Schwodiauer, I. Graz, S. Bauer-Gogonea, S. Bauer, T. Someya, *Nature* **2013**, *499*, 458.

[9] S. Kim, H. Y. Jeong, S. K. Kim, S. Y. Choi, K. J. Lee, *Nano Lett.* **2011**, *11*, 5438.

[10] G. M. Zhou, F. Li, H. M. Cheng, *Energy Environ. Sci.* **2014**, *7*, 1307.

[11] D. H. Kim, J. Z. Song, W. M. Choi, H. S. Kim, R. H. Kim, Z. J. Liu, Y. Y. Huang, K. C. Hwang, Y. W. Zhang, J. A. Rogers, *Proc. Natl. Acad. Sci. USA* **2008**, *105*, 18675.

[12] T. Someya, Y. Kato, T. Sekitani, S. Iba, Y. Noguchi, Y. Murase, H. Kawaguchi, T. Sakurai, *Proc. Natl. Acad. Sci. USA* **2005**, *102*, 12321.

[13] Z. Y. Fan, J. C. Ho, Z. A. Jacobson, H. Razavi, A. Javey, *Proc. Natl. Acad. Sci. USA* **2008**, *105*, 11066.

[14] D. J. Lipomi, M. Vosgueritchian, B. C. K. Tee, S. L. Hellstrom, J. A. Lee, C. H. Fox, Z. N. Bao, *Nat. Nanotechnol.* **2011**, *6*, 788.

[15] M. C. LeMieux, M. Roberts, S. Barman, Y. W. Jin, J. M. Kim, Z. N. Bao, *Science* **2008**, *321*, 101.

[16] Z. Q. Niu, L. L. Liu, L. Zhang, X. D. Chen, *Small* **2014**, *10*, 3434.

[17] D. P. Qi, Z. Y. Liu, Y. Liu, W. R. Leow, B. W. Zhu, H. Yang, J. C. Yu, W. Wang, H. Wang, S. Y. Yin, X. D. Chen, *Adv. Mater.* **2015**, *27*, 5559.

[18] B. W. Zhu, Z. Q. Niu, H. Wang, W. R. Leow, H. Wang, Y. G. Li, L. Y. Zheng, J. Wei, F. W. Huo, X. D. Chen, *Small* **2014**, *10*, 3625.

[19] Z. N. Bao, X. D. Chen, *Adv. Mater.* **2016**, *28*, 4177.

[20] Y. Tai, G. Lubineau, *Small* **2017**, *13*, 1603486.

[21] Y. Tai, G. Lubineau, *Sci. Rep* **2016**, *6*, 19632.

[22] M. C. Chen, C. L. Hsu, T. J. Hsueh, *IEEE Electron Device Lett.* **2014**, *35*, 590.

[23] H. C. Bi, K. B. Yin, X. Xie, J. Ji, S. Wan, L. T. Sun, M. Terrones, M. S. Dresselhaus, *Sci. Rep.* **2013**, *3*, 2714.

[24] S. Borini, R. White, D. Wei, M. Astley, S. Haque, E. Spigone, N. Harris, J. Kivioja, T. Ryhanen, *ACS Nano* **2013**, *7*, 11166.

[25] A. Ghosh, D. J. Late, L. S. Panchakarla, A. Govindaraj, C. N. R. Rao, *J. Exp. Nanosci.* **2009**, *4*, 313.

[26] T. S. MSreeprasad, A. A. Rodriguez, J. Colston, A. Graham, E. Shishkin, V. Pallem, V. Berry, *Nano Lett.* **2013**, *13*, 1757.

[27] H. C. Bi, K. B. Yin, J. Ji, S. Wan, L. T. Sun, M. Terrones, M. S. Dresselhous, *Sci. Rep.* **2013**, *3*, 2714.

[28] S. H. Hwang, D. W. Kang, R. S. Ruoff, H. S. Shin, Y. B. Park, *ACS Nano* **2014**, *8*, 6739.

[29] H. Schmidt, S. F. Wang, L. Q. Chu, M. Toh, R. Kumar, W. J. Zhao, A. H. C. Neto, J. Martin, S. Adam, B. Ozyilmaz, G. Eda, *Nano Lett.* **2014**, *14*, 1909.

[30] X. Cui, G. H. Lee, Y. D. Kim, G. Arefe, P. Y. Huang, C. H. Lee, D. A. Chenet, X. Zhang, L. Wang, F. Ye, F. Pizzocchero, B. S. Jessen, K. Watanabe, T. Taniguchi, D. A. Muller, T. Low, P. Kim, J. Hone, *Nat. Nanotechnol.* **2015**, *10*, 534.

[31] D. J. Late, B. Liu, H. S. S. R. Matte, V. P. Dravid, C. N. R. Rao, *ACS Nano* **2012**, *6*, 5635.

[32] S. L. Zhang, H. H. Choi, H. Y. Yue, W. C. Yang, *Curr. Appl. Phys.* **2014**, *14*, 264.

[33] D. J. Late, Y. K. Huang, B. Liu, J. Acharya, S. N. Shirodkar, J. J. Luo, A. M. Yan, D. Charles, U. V. Waghmare, V. P. Dravid, C. N. R. Rao, *ACS Nano* **2013**, *7*, 4879.

[34] J. Zhao, H. Yu, W. Chen, R. Yang, J. Q. Zhu, M. Z. Liao, D. X. Shi, G. Y. Zhang, *ACS Appl. Mater. Interfaces* **2016**, *8*, 16546.

[35] W. Chen, J. Zhao, J. Zhang, L. Gu, Z. Z. Yang, X. M. Li, H. Yu, X. T. Zhu, R. Yang, D. X. Shi, X. C. Lin, J. D. Guo, X. D. Bai, G. Y. Zhang, *J. Am. Chem. Soc.* **2015**, *137*, 15632.

[36] C. Lee, H. Yan, L. E. Brus, T. F. Heinz, J. Hone, S. Ryu, *ACS Nano* **2010**, *4*, 2695.

[37] Y. L. Wang, C. X. Cong, C. Y. Qiu, T. Yu, *Small* **2013**, *9*, 2857.

[38] S. Horzum, H. Sahin, S. Cahangirov, P. Cudazzo, A. Rubio, T. Serin, F. M. Peeters, *Phys. Rev. B* **2013**, *87*, 125415.

[39] K. F. Mak, K. L. He, C. Lee, G. H. Lee, J. Hone, T. F. Heinz, J. Shan, *Nat. Mater.* **2013**, *12*, 207.

[40] S. Tongay, J. Zhou, C. Ataca, J. Liu, J. S. Kang, T. S. Matthews, L. You, J. B. Li, J. C. Grossman, J. Q. Wu, *Nano Lett.* **2013**, *13*, 2831.

[41] J. O. Varghese, P. Agbo, A. M. Sutherland, V. W. Brar, G. R. Rossman, H. B. Gray, J. R. Heath, *Adv. Mater.* **2015**, *27*, 2734.

[42] Y. P. Dan, Y. Lu, N. J. Kybert, Z. T. Luo, A. T. C. Johnson, *Nano Lett.* **2009**, *9*, 1472.

[43] M. B. Erande, M. S. Pawar, D. J. Late, *ACS Appl. Mater. Interfaces* **2016**, *8*, 11548.

[44] J. Zhao, W. Chen, J. L. Meng, H. Yu, M. Z. Liao, J. Q. Zhu, R. Yang, D. X. Shi, G. Y. Zhang, *Adv. Electron. Mater.* **2016**, *2*, 1500379.